Red Blood Cell Membrane Dynamics during Malaria Parasite Egress

Andrew Callan-Jones,* Octavio Eduardo Albarran Arriagada, Gladys Massiera, Vladimir Lorman, and Manouk Abkarian*
Université Montpellier 2, Laboratoire Charles Coulomb UMR 5221, CNRS, Laboratoire Charles Coulomb UMR 5221, F-34095, Montpellier, France

ABSTRACT Precisely how malaria parasites exit from infected red blood cells to further spread the disease remains poorly understood. It has been shown recently, however, that these parasites exploit the elasticity of the cell membrane to enable their egress. Based on this work, showing that parasites modify the membrane's spontaneous curvature, initiating pore opening and outward membrane curling, we develop a model of the dynamics of the red blood cell membrane leading to complete parasite egress. As a result of the three-dimensional, axisymmetric nature of the problem, we find that the membrane dynamics involve two modes of elastic-energy release: 1), at short times after pore opening, the free edge of the membrane curls into a toroidal rim attached to a membrane cap of roughly fixed radius; and 2), at longer times, the rim radius is fixed, and lipids in the cap flow into the rim. We compare our model with the experimental data of Abkarian and co-workers and obtain an estimate of the induced spontaneous curvature and the membrane viscosity, which control the timescale of parasite release. Finally, eversion of the membrane cap, which liberates the remaining parasites, is driven by the spontaneous curvature and is found to be associated with a breaking of the axisymmetry of the membrane.

INTRODUCTION

Malaria is a devastating disease that affects up to 500 million people and kills over one million people each year (1). The causative agent of the deadliest form of malaria, the parasite *Plasmodium falciparum*, is a protozoan that is transmitted by mosquitoes to humans in the form of string-like sporozoites that attack the liver, multiply in liver cells, and then invade red blood cells in the form of micron-sized, droplet-shaped merozoites that infect the bloodstream. During the blood stage, a merozoite invades a healthy red blood cell (RBC); once inside, over a period of 48 h, it divides into 16–32 daughter merozoites by consuming the host hemoglobin; and finally, the merozoites exit the cell by piercing a hole in the plasma membrane, enabling them to continue infecting the bloodstream (2).

A long-standing, open question in the study of malaria is the nature of the release of merozoites from RBCs (3,4–6). Indeed, until very recently it had been accepted that parasite egress from rounded-up RBCs occurs explosively, presumably caused by osmotic-pressure-driven cell lysis (6). However, a recent work by Abkarian et al. has challenged this viewpoint, revealing that the release of merozoites may occur by a more programmed mechanism (3): first, a pore is created in the RBC membrane, allowing the first merozoites to exit; the pore then opens due to the outward curling of the membrane into a toroidal rim; and finally, the remaining merozoites are scattered by the eversion of the remaining membrane cap (see the video microscopy image sequence in Fig. 1). The curling and eversion of the RBC membrane, resulting in the complete egress of merozoites long after the initial swelling pressure in the cell has relaxed, strongly suggest a release mechanism of membrane elastic origin. It is still unknown, however, how parasites exploit membrane elasticity to effect their exit from RBCs. It is our goal here to describe the membrane dynamics of the RBC that lead to parasite egress.

Several studies indicate that malaria parasites induce modifications to the plasma membrane and its underlying spectrin cortex before egress (7–12). First, work on another malaria-causing parasite, *P. knowlesi*, revealed that merozoites alter the phospholipid asymmetry of the membrane bilayer of infected RBCs, inducing a relative enrichment of cone-shaped lipids, such as phosphatidylethanolamine, in the outer leaflet (7). Second, recent studies have shown that parasite-secreted proteases modify and degrade the spectrin cytoskeleton before egress (8–11) and that treatment with protease inhibitors prevents egress (13). Moreover, hijacking of the host protease calpain-1 by *P. falciparum* merozoites is essential to their egress from infected RBCs (12). Taken together, these studies and the observed membrane curling during parasite egress (3) suggest the following exit strategy: parasites induce a spontaneous curvature in the RBC membrane, opposite in sign to its mean curvature before their egress; to minimize the mismatch between the spontaneous curvature and the membrane curvature, a pore opens in the membrane, followed by outward membrane curling, and finally eversion. A similar mechanism has, in fact, been proposed to explain the bursting of polymersomes when stimulated by ultraviolet radiation (14). In recent theoretical work (15), Kabaso et al. have developed the idea that spectrin filaments that are only partially attached to the plasma membrane of

Submitted August 20, 2012, and accepted for publication November 5, 2012.
*Correspondence: andrew.callan-jones@univ-montp2.fr or Manouk.Abkarian@um2.fr
Editor: Charles Wolgemuth.

0006-3495/12/12/2475/9 $2.00
http://dx.doi.org/10.1016/j.bpj.2012.11.008

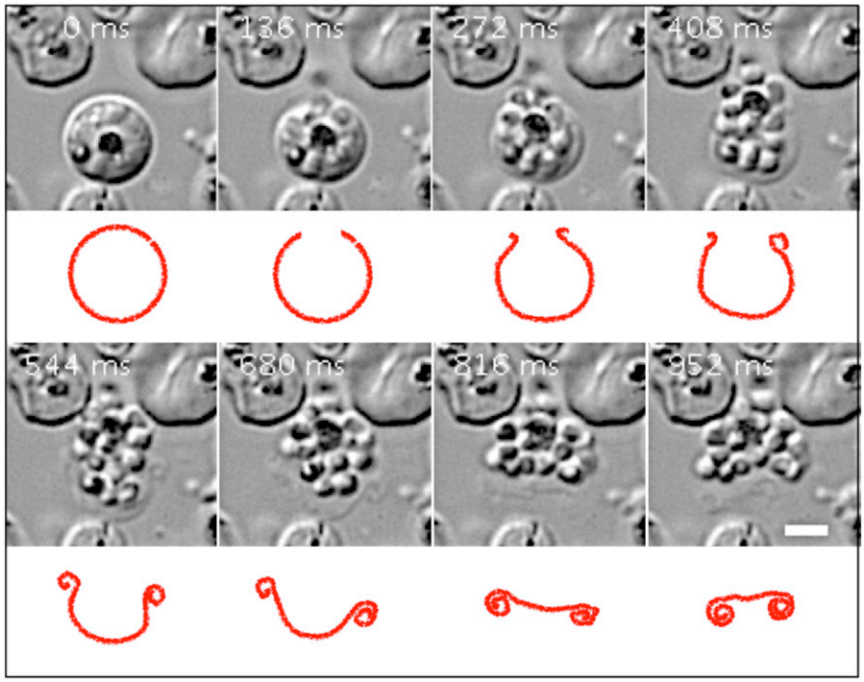

FIGURE 1 Merozoite egress from RBCs. Differential interference contrast microscopy reveals sequence of events leading to merozoite egress: a pore in the plasma membrane opens, allowing the first parasites to leave; next, the pore rim curls outward, causing further parasite escape; and finally, the remaining membrane cap everts, leading to complete egress.

a healthy RBC generate a spontaneous curvature, driving inside-out curling behavior, when the cell is placed in divalent cation-free medium (16).

In this article, we present a model of RBC membrane dynamics during merozoite egress resulting from the induced spontaneous curvature. Recognizing that malaria parasite egress is a vastly intricate process involving many biochemical actors, our objective is to shed some light on the geometry and mechanics of the RBC membrane that enable parasite escape. We focus on the elasticity of the plasma membrane, based on studies indicating that the structure of the spectrin cortex is significantly weakened before parasite egress (10,17,18). In contrast to earlier work on RBC membrane curling based on an elastic strip model (15), we have developed a three-dimensional, axisymmetric approach that takes into account the geometry of the RBC. We show that for geometric reasons, the membrane elastic energy is a nonmonotonic function of the pore-opening angle, and this has direct implications for the resulting membrane dynamics. In particular, these dynamics are characterized by a superposition of two types of movement: immediately after pore opening, curling of the membrane rim occurs while the membrane cap remains almost immobile; later, curling slows down, and feeding of material in the cap into the toroidal rim occurs to further release stored elastic energy. This process is illustrated in Fig. 2 *a*. Finally, cap eversion is understood as occurring as a result of the release of bending energy, which is favored by the induced spontaneous curvature.

Our article is organized as follows. We first outline the theoretical model used here, emphasizing the geometric and energetic aspects of the RBC membrane associated with parasite egress. We derive the elastic energy of the toroidal rim based on the bending energy of the RBC plasma

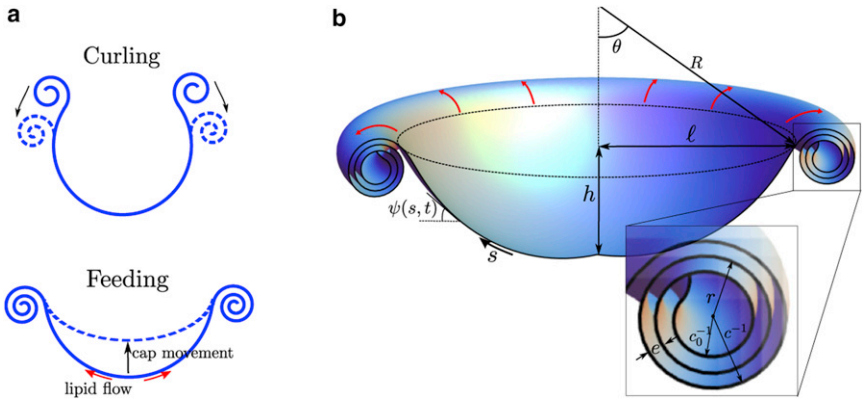

FIGURE 2 Illustration of membrane dynamics. (*a*) Curling of the membrane, starting at the free edge, occurs at early times after pore formation; feeding of the membrane cap into the rim occurs at later times. (*b*) At a given moment, the RBC membrane can be described as a toroidal rim connected to a spherical cap. The arrows around the rim represent the direction of lipid flow in the membrane during feeding; the changing direction of the lipid flow gives rise to surface viscous dissipation.

membrane with spontaneous curvature. We then develop coupled dynamical equations for curling and feeding based on the balancing of viscous dissipation with the release of elastic energy. We next present numerical results and fit our model to our experimental data, yielding an estimate of the induced spontaneous curvature. The comparison between our model and experimental data also reveal that viscous dissipation associated with surface lipid flows must be considered to explain the observed timescales in RBC membrane dynamics. In the Results section, we present a scaling analysis of the eversion step and explain the observed acceleration of the cap as it everts.

THEORY

The exit of malaria parasites from infected RBCs is a complex process involving biochemical changes to the cell membrane (8–11). In the theoretical description presented here, we model the cumulative effects of these changes by a spatially uniform spontaneous curvature, $-c_0$ ($c_0>0$). The consequences of this spontaneous curvature for RBC membrane dynamics have recently been studied experimentally (3); data analysis has revealed that the parasite-induced spontaneous curvature is $c_0 = 10 - 20\ \mu\text{m}^{-1}$.

After pore opening in the RBC membrane, the spontaneous curvature, c_0, drives outward curling of the plasma membrane starting at the pore edge. Comparing the measured values of c_0^{-1} with the radius, R_0, of the spherical RBC before egress, equal to ~3 μm (3), the largeness of the parameter c_0R_0 permits a simple decomposition of the RBC membrane as follows: at any moment during parasite egress, the RBC membrane is assumed to consist of a spherical cap of radius $R(t)$, opening angle $\theta(t)$, and depth $h(t) = R(1-\cos\theta)$, attached to a toroidal rim of major radius given approximately by $\ell(t) = R\sin\theta$; see Fig. 2 *b*. The rim is assumed to consist of concentric tori, each separated by a distance e. Based on the assumption $c_0R_0 \gg 1$, the mean curvature, H, at a point on an inner torus of minor radius r and major radius ℓ is dominated by $1/r$, and thus $H \approx 1/(2r)$; by the condition of zero moment at the free edge, the minor radius of the innermost torus is $\sim c_0^{-1}$ (19).

The minor radius of the outermost torus is denoted as c^{-1}. It is assumed in this study that the total RBC membrane area is conserved during egress, which directly yields the dependence of c^{-1} on θ and R: equating the area of the initially spherical RBC of radius R_0 and opening angle θ_0 (right after pore nucleation) to the area of the cap of radius R and opening angle θ plus the total area contained in the rim yields

$$2\pi R_0^2(1-\cos\theta_0) = 2\pi R^2(1-\cos\theta) + \int_{c_0^{-1}}^{c^{-1}} 2\pi R\sin\theta \times 2\pi r\frac{dr}{e}. \quad (1)$$

In Eq. 1, dr/e counts the number of tori over a distance dr; the condition $c_0R_0 \gg 1$ leads to the simplifying assumption that as the angle θ varies, there is an integral number of tori in the rim. Simplification of the above equation yields

$$c^{-1}(\theta,R) = c_0^{-1}\sqrt{1+\frac{\beta}{\sin\theta}\left(\frac{R_0}{R}(1-\cos\theta_0) - \frac{R}{R_0}(1-\cos\theta)\right)}, \quad (2)$$

where $\beta = eR_0c_0^2/\pi$ is a geometric parameter of the order of 5–10 (3). In the next section, we use the arguments described here to derive the elastic energy released by formation of the rim.

ENERGY OF THE MEMBRANE RIM

We demonstrate here that, as a result of the axisymmetry of the problem, the elastic energy of the membrane during egress depends nonmonotonically on the cap opening angle, θ. This result will be shown to imply two dynamical regimes during egress: a curling regime at early times and a feeding regime at late times.

The energy of the RBC membrane at a given moment during egress is composed of three terms: the Helfrich bending energy of the toroidal rim of area, A_{rim}; the line energy associated with the free membrane edge; and the Helfrich bending energy of the membrane cap of radius R and area A_{cap}. This last term can be neglected, because for $c_0R_0 \gg 1$, it is, at leading order, equal to $F_{\text{cap}} = \kappa c_0^2 A_{\text{cap}}/2$, where κ is the membrane bending stiffness; since a similar term, $\kappa c_0^2 A_{\text{rim}}/2$, arises in the energy of the rim, because of the assumed constancy of $A_{\text{cap}} + A_{\text{rim}}$, terms proportional to c_0^2 amount to an additive constant and thus can be neglected. We note that we do not consider the elastic energy associated with the spectrin cortex, as justified earlier.

The energy released into the rim, given by the bending energy $\kappa/2\int_{\text{rim}}(4H^2 - 4c_0H)dA$ and a contribution from the line tension, γ, of the free edge, is, for given θ, R, and $c_0R_0 \gg 1$, equal to

$$\begin{aligned} F_{\text{rim}} &= \frac{\kappa}{2}\int_{c_0^{-1}}^{c^{-1}}\left(\frac{1}{r^2} - \frac{2c_0}{r}\right)2\pi R\sin\theta \times 2\pi r\frac{dr}{e} + 2\pi\gamma R\sin\theta \\ &= \frac{2\pi^2\kappa R}{e}\sin\theta\left[\ln\left(\frac{c_0}{c}\right) - 2\left(\frac{c_0}{c} - 1\right) + \tilde{\gamma}\right], \end{aligned} \quad (3)$$

where $\tilde{\gamma} = \gamma e/(\pi\kappa)$. For a bare lipid membrane of bilayer thickness α, $\gamma = \pi\kappa/a$ (20), and thus $\tilde{\gamma} = e/a \approx 10$, where we have taken $e \approx 50$ nm (21) and $a \approx 5$ nm (22). However, curved membrane proteins localized at the membrane edge are known to stabilize it (20), thus reducing $\tilde{\gamma}$; we take $\tilde{\gamma}$ to be on the order of 1. For simplicity, we did not consider the

contribution of the Gaussian curvature, K, integrated over the entire cell membrane, to the bending energy. We note that, according to the Gauss-Bonnet theorem, $\int_{\text{cell}} K dA = 2\pi - \oint_{\text{edge}} \kappa_g dl$, where the second term on the right is the geodesic curvature, κ_g, integrated over the free edge of the membrane (23). However, $\kappa_g \approx \cos\psi(s_{\text{edge}}, t)/\ell$, where the angle $\psi(s,t)$, depending on the arc length parameter s and time t, is defined in Fig. 2 *b*; thus, the Gaussian curvature simply contributes an oscillating term to the energy that averages to zero on the timescales that interest us here, i.e., greater than the time needed for the rim to complete a turn.

PARASITE EGRESS REQUIRES CURLING AND FEEDING

To highlight the influence of geometry on membrane dynamics, for the moment we consider $R(t) = R_0$ and $\theta_0 = \pi$, and examine how F_{rim} depends on the angle θ.

With these simplifications, the rim minor radius is given by $c^{-1}(\theta) = c_0^{-1}\sqrt{1 + \beta\cot(\theta/2)}$; inserting this into Eq. 3. yields

$$F'_{\text{rim}} = \frac{2\pi^2\kappa R_0}{e}\sin\theta\left[\frac{1}{2}\ln(1+\beta\cot(\theta/2)) - 2\left(\sqrt{1+\beta\cot(\theta/2)} - 1\right) + \tilde{\gamma}\right], \tag{4}$$

where $F'_{\text{rim}} = F_{\text{rim}}|_{\{R=R_0,\ \theta_0=0\}}$. Fig. 3 reveals the dependence of the rim energy, F'_{rim}, on the opening angle, θ. The maximum in the energy near $\theta = \pi$ reflects the pore nucleation barrier resulting from a competition between the energetic drive for pore opening due to the spontaneous curvature and the opposing tendency of the pore line tension

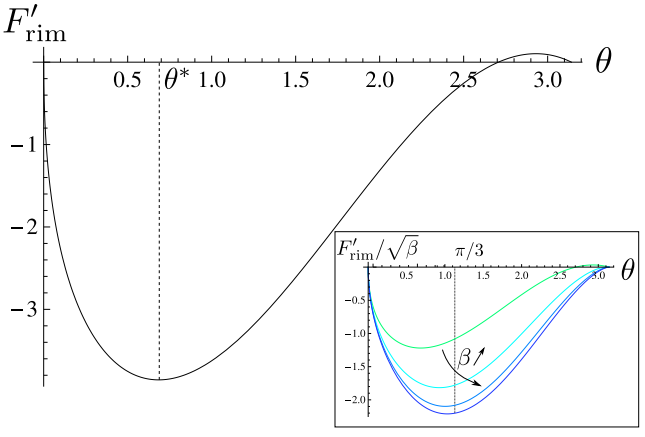

FIGURE 3 The rim energy, F'_{rim}, as a function of pore opening angle. F'_{rim} is plotted in units of $2\pi^2\kappa R_0/e$ and θ is in rads. The maximum in F'_{rim} near $\theta = \pi$ represents the nucleation barrier for pore opening; the minimum is a result of axisymmetry of the problem, and indicates that pure curling will stop near $\theta = \theta^*$. Parameter values: $\beta = 10$ and $\tilde{\gamma} = 1$. (*Inset*) $F'_{\text{rim}}/\sqrt{\beta}$ versus θ for $\beta = 10$, 100, 1000, and 10,000, illustrating the convergence of θ^* toward $\pi/3$.

(14). Interestingly, there is a minimum in the energy for $\theta = \theta^*$, which is a direct consequence of the three-dimensional curling geometry: since F'_{rim} is proportional to the rim radius, $\ell = R_0\sin\theta$, curling will slow down and then stop as ℓ decreases, since less and less elastic energy is released into the rim. This finding is a key result of this work, and will play an important role in the opening dynamics of the membrane leading to parasite egress. Due to this geometric effect, three-dimensional curling of a membrane is intrinsically different from the curling of an elastic strip with natural curvature (24–26, and (O. Albarran, G. Massiera, and M. Abkarian, unpublished)), a model for red blood cell membrane curling used previously (15). After the curling stops, further elastic energy can be released by flows of lipids in the cap into the rim.

The minimum angle, θ^*, can be determined easily for $\beta \gg 1$, in which case $F'_{\text{rim}} \sim -2\sin\theta\sqrt{\beta\cot(\theta/2)}$; minimization with respect to θ results in $\theta^* \approx \pi/3$. Fig. 3 shows that θ^* increases with β and converges to $\pi/3$. We note that the curling arrest angle θ^* increases with c_0. One might expect that the larger the c_0 the more the rim would curl up, but this is not true, since greater curling would imply a smaller ℓ, thus releasing less elastic energy.

MEMBRANE DYNAMICS

The minimum in the rim elastic energy as a function of opening angle suggests that the membrane dynamics during parasite egress are nontrivial, and that they require membrane curling and feeding. In this section, based on the rim energy derived earlier, we develop a model describing the coupled curling and feeding dynamics that enables complete parasite egress.

Pure curling of the membrane consists of the pore opening while the cap radius, R, remains constant. Feeding, on the other hand, involves transport of lipid material from the cap into the rim while the rim radius ℓ remains constant. The low Reynolds' number curling dynamics is described by equating the rate of elastic energy released during curling with the power dissipated by the movement of the toroidal rim (14). This power contains two contributions: a bulk term due to rim movement with respect to the background solvent, and a surface term due to axisymmetric lipid flows in the plane of the membrane. First, the bulk term is approximated here by the Stokes friction due to motion of a cylinder of length $2\pi\ell$ and radius $\sim c_0^{-1}$ moving at a speed $v = -R\dot{\theta}$, where an overdot denotes a time derivative. The frictional force on such a cylinder moving perpendicularly to its axis at speed v is $f_\perp = 8\pi^2\eta_0\ell v/(\ln(2\pi\ell c_0) + (1/2))$, where η_0 is the viscosity of the medium (28). The bulk power dissipated, $P_{bc} = f_\perp v$, is thus $P_{bc} \approx 2\pi\ell(4\pi/l_n)\eta_0 v^2$, where $l_n = \ln(2\pi\ell c_0) + (1/2)$ depends weakly on ℓ. Second, the surface term is $P_{sc} \approx \eta_s A_{\text{rim}}(v/\ell)^2$, where η_s is the membrane viscosity. Noting that $A_{\text{rim}} = (2\pi^2\ell/e)(c^{-2} - c_0^{-2})$, curling is described by the equation

$$\dot{F}_{\rm rim}\big|_R + 2\pi^2\ell\left(\frac{4\eta_0}{l_n} + \left(\frac{1}{c^2} - \frac{1}{c_0^2}\right)\frac{\eta_s}{\ell^2 e}\right)(R\dot{\theta})^2 = 0, \qquad (5)$$

where the subscript R means that the derivative is taken at constant R. The full expression of $\dot{F}_{\rm rim}|_R$ is found in the appendix.

The dynamical equation describing feeding is obtained by balancing the elastic energy released by transferring membrane from the weakly curved cap into the rim with the power dissipated by movement of the cap and by in-plane lipid flow. Denoting the total membrane area as A and the velocity of lipids flowing into the rim as v_s, the feeding dynamics are thus described approximately by

$$\dot{F}_{\rm rim}\big|_\ell + \pi\eta\left(\frac{\dot{h}\big|_\ell}{\lambda}\right)^2\lambda^3 + \eta_s A\left(\frac{v_s}{\ell}\right)^2 = 0, \qquad (6)$$

where the subscript ℓ means that the derivative is taken with the rim radius ℓ constant. We emphasize here that due to the geometric complexity of the problem, the dissipative terms in Eq. 6 are approximate, and that geometrical coefficients have been absorbed into the definitions of the viscosities η and η_s (28). The full expressions of $\dot{F}_{\rm rim}|_\ell$, $\dot{h}|_\ell$, and v_s are found in the appendix. In Eq. 6, λ is a characteristic length over which dissipation occurs, given by $\lambda \approx \sqrt{A_{\rm cap}} = \sqrt{2\pi R^2(1-\cos\theta)}$. We note that the viscosity of the fluid surrounding the cap, η, is different than the solvent viscosity, η_0. We assume that the solvent and the merozoites that are pushed forward by the cap behave as a colloidal suspension with a viscosity that may be as much as 10–100 times η_0, depending on the volume fraction of merozoites (29).

RESULTS

Curling and feeding

The solution to the coupled dynamical equations (Eqs. 5 and 6) yields the time evolution of the opening angle, $\theta(t)$, and the cap radius, $R(t)$. Fig. 4 *a* illustrates the solutions $\theta(t)$ and $R(t)$, and reveals that the membrane dynamics consist of two distinct regimes. At early times after pore opening, membrane curling occurs, during which the opening angle, $\theta(t)$, changes markedly, whereas the cap radius $R(t)$ remains almost constant. Note that this latter result justifies a posteriori the approximation $R(t) = R_0$ in the analysis leading to Eq. 4. At longer times, feeding dominates, during which $\theta(t)$ decreases slowly and $R(t)$ increases, causing a flattening of the cap. This behavior is further supported by Fig. 4 *b*, which shows the cap depth, h, and the number of turns in the rim, $N = (c^{-1} - c_0^{-1})/e$, as functions of time. We note that N increases rapidly during the curling regime and levels off during feeding.

The trends represented in Fig. 4 indicate, however, that the clear separation between curling and feeding may be blurred by the effects of membrane surface viscosity, since curling is slowed down by in-plane viscous shear stresses involved in toroidal rotation. In fact, if one neglects the surface viscosity, the characteristic time associated with curling, $\eta_0/(\kappa c_0^3)$, is less than a millisecond, assuming $\eta_0 = 10^{-3}$ Pa•s (viscosity of water), $\kappa = 50\ k_{\rm B}T$ (30), and $c_0 = 10\ \mu{\rm m}^{-1}$. This time is too small to explain the curling dynamics observed in Abkarian et al. (3) that occur on the order of tens of milliseconds. Moreover, comparison of our model with membrane dynamics during parasite egress from RBCs suggests that membrane viscous stresses may be the dominant dissipative mode. Indeed, fitting our experimental data for $h(t)$ with our model, we obtain $c_0 \approx 10\ \mu{\rm m}^{-1}$ and $\eta_s/\eta_0 \approx 1000\ \mu$m (see Fig. 5). The value of the fit parameter c_0 is consistent with an earlier measurement (3). For infected RBCs, we find, based on the values of c_0 and η_s, that the ratio of surface to bulk dissipation, given approximately by $\eta_s/(\eta_0 e\ell^2 c_0^2)$, is $\gg 1$. Here, we have taken $\ell \approx 1\ \mu$m and $e = 50$ nm (3); in addition, in obtaining our fit parameters, we have taken $\eta = 100\eta_0$. This choice reflects the contribution of the merozoites to the bulk

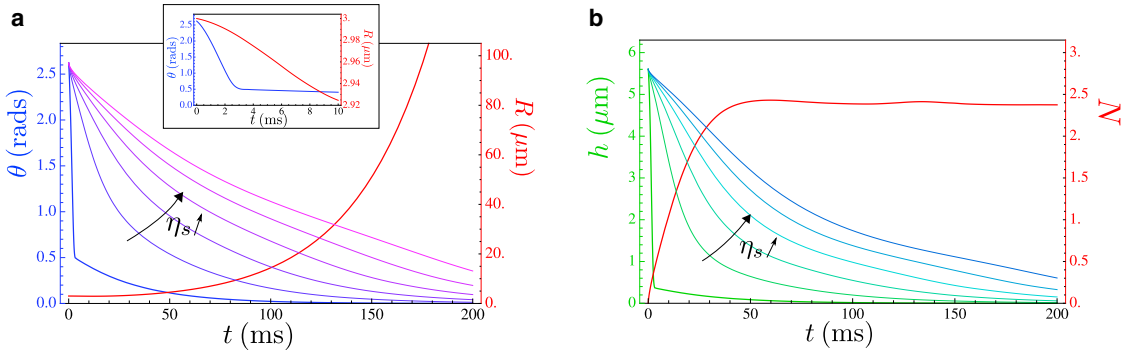

FIGURE 4 Membrane dynamics during parasite egress. (*a*) The pore opening angle, θ, and cap radius, R, versus t. θ is shown for different values of the ratio of surface to bulk viscosities, η_s/η_0, ranging from 0 to 500 μm, in increments of 100 μm. R is shown for $\eta_s/\eta_0 = 100\ \mu$m. (*Inset*) Zoom of the early time behavior. θ is shown for $\eta_s = 0$, revealing a smooth change from curling to feeding. R is shown for $\eta_s/\eta_0 = 100\ \mu$m, showing a small decrease, expected initially during feeding based on the geometry. The other parameter values are $c_0 = 10\ \mu{\rm m}^{-1}$, $R_0 = 3\ \mu$m, $e = 0.05\ \mu$m, $l_n = 5$, $\kappa/\eta_0 = 0.2\ \mu{\rm m}^3/{\rm ms}$, $\tilde{\gamma} = 1$, and $\eta/\eta_0 = 100$. (*b*) The cap depth, h, and number of turns in the rim, N, versus t. h is shown for different values of the surface/bulk viscosity ratio, η_s/η_0, ranging from 0 to 500 μm, in increments of 100 μm. N is shown for $\eta_s/\eta_0 = 100\ \mu$m. The other parameters are the same as in *a*.

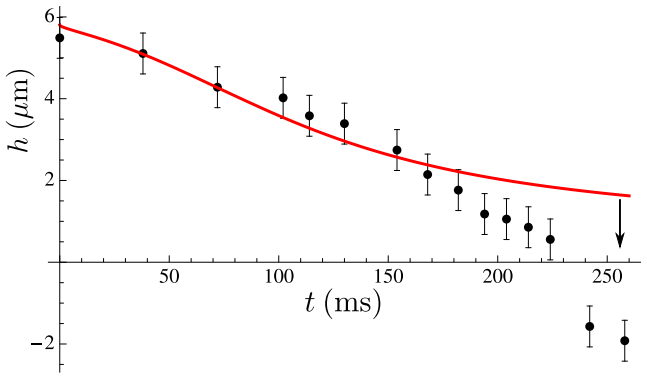

FIGURE 5 Model fit to experimental results. The cap depth, h, versus t during parasite egress from RBCs. Data from Abkarian et al. (1) (*circles*) is fitted with the model developed in this work. The fit parameters are $c_0 = 13 \pm 4\ \mu\text{m}^{-1}$ and $\eta_s/\eta_0 = 1400 \pm 400\ \mu\text{m}$. Deviation between the data and the model is expected for small h; the arrow indicates the expected shift in the model when the constraint of axisymmetry is relaxed (see text). The other, fixed parameters are: $R_0 = 3\ \mu\text{m}$, $e = 0.05\ \mu\text{m}$, $l_n = 5$, $\kappa/\eta_0 = 0.2\ \mu\text{m}^3/\text{ms}$, $\tilde{\gamma} = 1$, and $\eta/\eta_0 = 100$.

viscous dissipation during cap movement. Nonetheless, we found that the values of c_0 and η_s/η_0 are largely insensitive to η: a 50% change in η results in changes in c_0 and η_s/η_0 of $<1\%$. Finally, to avoid the proliferation of too many fit parameters, we have fixed those, such as κ, e, and γ, that are reasonably well known, and have only kept as trial parameters those related to the RBC membrane that are susceptible to modification by the parasites, i.e., c_0 and η_s/η_0.

From Fig. 5, it is apparent that agreement between our theoretical model and the experimental values of the cap depth, $h(t)$, breaks down at long times, at which $h(t)$ rapidly passes through zero and changes sign. In fact, Abkarian and co-workers (3) have shown that the final step of parasite egress from RBCs involves an eversion of the membrane cap, leading to dispersal of the last parasites (3) (see the last frame of Fig. 1). Similar eversion behavior was also observed in the last stages of polymersome bursting (14).

Eversion of the membrane cap

Eversion can be understood based on the energetic drive of the induced spontaneous curvature to reverse the initial curvature of the infected RBC. However, as we have shown, energetic and geometric requirements imply that curling and feeding pin the rim radius at a certain value ℓ^*. (The rim radius, ℓ^*, can be estimated via minimization of F'_{rim} (Eq. 4) with respect to θ. As a result, $\ell^* = R_0 f(\beta, \tilde{\gamma})$, where f is a dimensionless function. For $\beta \gg 1$, we find $\theta^* \approx \pi/3$ and, therefore, $\ell^* \approx \sqrt{3}R_0/2$.) This means that for the cap to evert and at the same time maintain a fixed amount of material in the rim, the axisymmetry of the rim and cap must be broken. Eversion thus allows the cap to be bent strongly along one direction, reducing the mismatch between the mean cap and spontaneous curvatures; this is illustrated in Fig. 6, in which, for simplicity, the cap bends principally along the x-direction.

Scaling arguments can be made to shed some light on cap eversion. Referring to Fig. 6, on the one hand, the energy released by eversion is $\delta F_{\text{cap}} \sim \kappa c_0 h$. (We neglect the bending term, $\sim \kappa h^2/\ell^{*2}$, since its contribution to the dynamics, $\sim \kappa h\dot{h}/\ell^{*2}$, is of an order $1/(\ell^* c_0)^2$ smaller than the feeding term, $\kappa c_0^2 h\dot{h}$.) On the other hand, the typical lateral displacement of the rim due to eversion is $u \sim h^2/\ell^*$, and therefore the energy penalty in deforming the rim is of the order h^4. Thus, the membrane cap dynamics for small $|h|$ can be understood by comparing the rate of energy released during feeding and eversion, given by $\sim -\kappa c_0^2 \ell^* v_s + \kappa c_0 \dot{h} \sim \kappa c_0^2 h\dot{h} + \kappa c_0 \dot{h}$, with the power dissipated $P \sim \eta_s v_s^2 + \eta \ell^* \dot{h}^2 \sim \eta_s (h\dot{h}/\ell^*)^2 + \eta \ell^* \dot{h}^2$. Here, we note that, according to the relation $\dot{A}_{\text{cap}} = -2\pi\ell^* v_s = 2\pi h\dot{h}$, $v_s = -h\dot{h}/\ell^*$ for $|h|/\ell^* \ll 1$. Thus, we obtain

$$\dot{h} \approx -\frac{\kappa c_0}{\eta \ell^* + \eta_s \dfrac{h^2}{\ell^{*2}}}(1 + h c_0). \tag{7}$$

Equation 7 indicates that for $|hc_0| \lesssim 1$, feeding of cap material into the rim cannot keep up with the drive for eversion. This might explain the apparent swelling of the rim and the appearance of broad shoulders in the membrane connecting the cap and rim just before eversion, seen in both Abkarian et al. (3) and Mabrouk et al. (14). It is important to note that Eq. 7 reveals that the total viscous resistance decreases as $|h|$ decreases, thereby explaining the observed acceleration of the cap during eversion (see Fig. 5). Indeed, for small $|h|$, we obtain

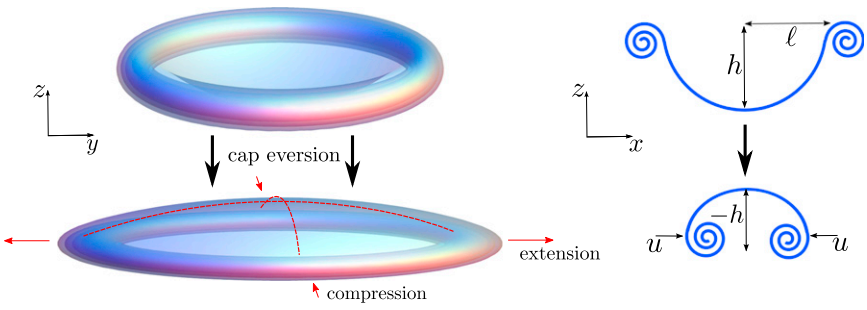

FIGURE 6 Final stage of parasite egress: eversion of the cap. As feeding ends, further elastic energy can be released by everting the cap, thus breaking the axisymmetry. For clarity, after eversion, the cap bends mainly along the x-direction. Eversion leads to a lateral displacement of the rim, denoted u.

$$h(t) \approx \left(\frac{-3\kappa c_0 \ell^{*2} t}{\eta_s} \right)^{1/3}, \quad (8)$$

with $t = 0$ being the moment that h passes through zero. Equation 8, another important product of our work, suggests that merozoites may exploit the RBC geometry to facilitate the final stage of egress. A more quantitative study of eversion will be considered in subsequent work.

DISCUSSION

An unresolved problem in the study of malaria infection is the mechanism by which parasites exit red blood cells, thereby transmitting the disease in the bloodstream. Motivated by recent work on the transmission mechanism (1,6,9,12,18), and inspired by modeling of bursting polymersomes (14), we have developed a theoretical description of the membrane energetics and dynamics that enable parasite egress from infected RBCs. Starting from the experimental observation that parasites induce a spontaneous curvature in the RBC plasma membrane before egress, driving pore formation and outward curling of the membrane (3), our model makes qualitative and quantitative predictions for the membrane dynamics leading to egress.

The main theoretical finding of our work is that the RBC membrane dynamics during parasite egress consist of a superposition of two types of membrane movement: 1), curling of the membrane into a toroidal rim that dominates at short times after pore opening; and 2), feeding of the remaining membrane cap into the rim at long times. This division stems from the axisymmetric character of the RBC membrane, implying a nonmonotonic dependence of the rim elastic energy on the pore opening angle. We found, however, that surface viscous dissipation, which slows down curling, can obscure the separation between curling and feeding. In fact, to explain the membrane dynamics involved in parasite egress from RBCs, observed experimentally, we determined that surface dissipation dominates bulk dissipation. By fitting our model to experimental depth data, we found that $c_0 \approx 10\ \mu\text{m}^{-1}$, in agreement with earlier findings (1). In addition, we found that the lengthscale below which surface dissipation dominates bulk dissipation, η_s/η_0, is on the order of 1 mm. Interestingly, this value is much larger than one would expect by naïvely assuming a value of $\eta_s \approx 10^{-9}$ Pa·s·m (yielding $\eta_s/\eta_0 = 1\ \mu$m for $\eta_0 = 10^{-3}$ Pa·s), typical for a lipid membrane (33). The membrane viscosity of malaria-infected RBCs is not known; however, our fit value is comparable to viscoelastic relaxation measurements on healthy RBCs, yielding $\eta_s = 10^{-6}$ Pa·s·m (34). This suggests that during malaria egress, the RBC membrane, though modified by parasites (7–12), is populated by spectrin filaments and other large proteins.

The approach developed here is based on the wide separation of two length scales: the RBC radius, R_0, and the inverse spontaneous curvature, c_0^{-1}. In our model, the inequality $c_0 R_0 \gg 1$ allows a division of the membrane into a toroidal rim attached to a spherical cap. The membrane dynamics are thus described in terms of the coupled motions of the rim and the cap, obtained by balancing elastic energy released with viscous dissipation due to the respective movements. Using this straightforward approach, we were able to identify differences between three-dimensional membrane curling and curling of an elastic strip and the key physical parameters enabling parasite egress. We note that an alternative approach would be to attempt to solve exactly (and numerically) the coupled elastohydrodynamical equations describing the relaxation of a membrane with spontaneous curvature in a viscous fluid. Given that the dynamics of a weakly fluctuating RBC membrane in a viscous medium is already a nontrivial problem (35–37), it is not clear whether an exact approach to the membrane dynamics leading to parasite egress, which involve geometric elastic nonlinearities coupled to flows, would be feasible or, for that matter, would provide more physical understanding than the approach we have pursued here.

Finally, we point out directions for further investigation into the mechanism of malaria parasite egress from RBCs. In this work we have not considered the elastic energy associated with the spectrin cortex. Nonetheless, it is worthwhile to compare the cortical elastic energy with the membrane bending energy. The energy scale associated with cortical stretching is $K_\alpha R_0^2$, where K_α is the (2D) area expansion modulus. Assuming for the moment that the cortex is intact, $K_\alpha \approx 9 \times 10^{-6}$ N/m (38). Taking $R_0 = 3\ \mu$m, the typical stretching energy is on the order of 10^{-16} J. On the other hand, the energy scale associated with the release of membrane bending energy due to the spontaneous curvature, c_0, is $\kappa R_0 c_0 (R_0/e)^{1/2}$ (this energy scale is obtained by considering the large β limit of Eq. 4). Taking $\kappa = 50 k_B T$, $c_0 = 10\ \mu\text{m}^{-1}$, and $e = 50$ nm, the typical membrane energy scale is also 10^{-16} J. Thus, if the spectrin cortex is intact, as in a healthy RBC, the stretching energy is at most of the same order of magnitude as the elastic energy of the membrane. However, several studies indicate that the spectrin cortex is compromised before malaria parasite egress, which would suggest that the cortical elastic moduli are lower than their values for healthy RBCs (8–12). Consistent with these observations, we have neglected the elastic contribution of the spectrin cortex. Future work is needed, however, to understand to what extent the cortex is modified before parasite egress. A related problem is the origin of the membrane surface dissipation entering into our model via the viscosity, η_s. This quantity could be probed by micropipette-based viscolelastic relaxation measurements on infected RBCs. We note that stretching of a partially intact spectrin cortex would slow down the membrane dynamics leading to egress; including such an effect in an extended model would result in a lower estimation of η_s. We have

shown that the surface viscous resistance to the flattening of the RBC membrane cap and its eversion decreases as the cap flattens. Thus, an issue that merits further consideration is whether parasites exploit this geometric effect during feeding; if so, can malaria egress be slowed down by arresting the membrane dynamics once curling has ended?

APPENDIX: DYNAMICAL EQUATIONS FOR CURLING AND FEEDING

To derive the dynamical equation describing curling, we start from the energy balance (Eq. 5). Then, calculating $dF_{\rm rim}/dt|_R$ using Eq. 3, we obtain the curling equation

$$\dot\theta + \frac{\kappa}{4eR^2\left(\frac{\eta_0}{l_n} + \left(\frac{1}{c^2} - \frac{1}{c_0^2}\right)\frac{\eta_s}{4\ell^2 e}\right)}\left\{\cot\theta\left[\ln\left(\frac{c_0}{c}\right) - 2\left(\frac{c_0}{c} - 1\right) + \tilde\gamma\right] - \frac{\partial c}{\partial\theta}\left(\frac{1}{c} - \frac{2c_0}{c^2}\right)\right\} = 0. \tag{9}$$

In this equation, c is given by Eq. 2.

To find the dynamical equation describing feeding, we consider the balance equation, Eq. 6. Noting that $\dot\theta|_\ell = -\tan\theta\dot R/R$, which yields, using Eq. 1,

$$\dot c|_\ell = \frac{ec^3\dot R}{2\pi}(2\tan(\theta/2) - \tan\theta), \tag{10}$$

we find the rate of change of energy:

$$\begin{aligned}\dot F_{\rm rim}\big|_\ell &= \frac{2\pi^2\kappa\ell\dot c|_\ell}{e}\left(\frac{2c_0}{c^2} - \frac{1}{c}\right)\\ &= \pi\kappa\ell c^2\dot R\left(\frac{2c_0}{c} - 1\right)(2\tan(\theta/2) - \tan\theta).\end{aligned} \tag{11}$$

The dissipation consists of two terms. Noting that $\dot h|_\ell = \dot R(1 - \sec\theta)$ and $\lambda = \sqrt{2\pi R^2(1-\cos\theta)}$, the bulk power dissipated by cap movement during feeding is

$$P_{fb} = \pi\eta\sqrt{2\pi(1-\cos\theta)}(1-\sec\theta)^2R\dot R^2. \tag{12}$$

The surface dissipation, $P_{fs} = \eta_s A(v_s/\ell)^2$, is found as follows. The velocity of lipids flowing into the rim during feeding, v_s, is related to the time derivative of the cap area: $\dot A_{\rm cap}|_\ell = -2\pi\ell v_s$, which yields $v_s = -\dot R(2\tan(\theta/2) - \tan\theta)$ and therefore

$$P_{fs} = \eta_s A(2\tan(\theta/2) - \tan\theta)^2\left(\frac{\dot R}{\ell}\right)^2. \tag{13}$$

Combining Eqs. 11–13, we thus obtain the feeding equation

$$\dot R + \frac{\kappa c^2}{\left(\eta + \frac{2R_0^2(1-\cos\theta_0)(2\tan(\theta/2)-\tan\theta)^2}{R\ell^2\sqrt{2\pi(1-\cos\theta)}(1-\sec\theta)^2}\eta_s\right)}\left(\frac{2c_0}{c} - 1\right)\frac{\sin\theta(2\tan(\theta/2)-\tan\theta)}{\sqrt{2\pi(1-\cos\theta)}(1-\sec\theta)^2} = 0. \tag{14}$$

Equations 9 and 14, along with Eq. 2, can then be solved for $\theta(t)$ and $R(t)$, given initial conditions $\theta(0) = \theta_0$ and $R(0) = R_0$.

We would like to thank Patricia Bassereau for a careful reading of the manuscript. A.C.-J. acknowledges useful discussions with Jérôme Dorignac.

This work was supported by funding from the Interdisciplinary Program of Université Montpellier 2 and the Languedoc-Roussillon region. UMR 5221 belongs to the CNRS French Consortium CellTiss.

REFERENCES

1. http://www.ncbi.nlm.nih.gov/pubmedhealth/PMH0001646/.
2. Understanding Malaria. Information booklet. http://health.nih.gov/topic/Malaria.
3. Abkarian, M., G. Massiera, …, C. Braun-Breton. 2011. A novel mechanism for egress of malarial parasites from red blood cells. *Blood.* 117:4118–4124.
4. Dvorak, J. A., L. H. Miller, …, T. Shiroishi. 1975. Invasion of erythrocytes by malaria merozoites. *Science.* 187:748–750.
5. Trager, W. 2002. On the release of malaria merozoites. *Trends Parasitol.* 18:60–61.
6. Glushakova, S., D. Yin, …, J. Zimmerberg. 2005. Membrane transformation during malaria parasite release from human red blood cells. *Curr. Biol.* 15:1645–1650.
7. Gupta, C. M., and G. C. Mishra. 1981. Transbilayer phospholipid asymmetry in *Plasmodium knowlesi*-infected host cell membrane. *Science.* 212:1047–1049.
8. Blisnick, T., M. E. Morales Betoulle, …, C. Braun Breton. 2000. Pfsbp1, a Maurer's cleft *Plasmodium falciparum* protein, is associated with the erythrocyte skeleton. *Mol. Biochem. Parasitol.* 111:107–121.
9. Salmon, B. L., A. Oksman, and D. E. Goldberg. 2001. Malaria parasite exit from the host erythrocyte: a two-step process requiring extraerythrocytic proteolysis. *Proc. Natl. Acad. Sci. USA.* 98:271–276.
10. Dhawan, S., M. Dua, …, M. Hanspal. 2003. Ankyrin peptide blocks falcipain-2-mediated malaria parasite release from red blood cells. *J. Biol. Chem.* 278:30180–30186.
11. Lanzer, M., H. Wickert, …, C. Braun Breton. 2006. Maurer's clefts: a novel multi-functional organelle in the cytoplasm of *Plasmodium falciparum*-infected erythrocytes. *Int. J. Parasitol.* 36:23–36.
12. Chandramohanadas, R., P. H. Davis, …, D. C. Greenbaum. 2009. Apicomplexan parasites co-opt host calpains to facilitate their escape from infected cells. *Science.* 324:794–797.
13. Chandramohanadas, R., Y. Park, …, S. Suresh. 2011. Biophysics of malarial parasite exit from infected erythrocytes. *PLoS ONE.* 6:e20869.
14. Mabrouk, E., D. Cuvelier, …, M. H. Li. 2009. Bursting of sensitive polymersomes induced by curling. *Proc. Natl. Acad. Sci. USA.* 106:7294–7298.
15. Kabaso, D., R. Shlomovitz, …, N. S. Gov. 2010. Curling and local shape changes of red blood cell membranes driven by cytoskeletal reorganization. *Biophys. J.* 99:808–816.
16. Lew, V. L., A. Hockaday, …, R. M. Bookchin. 1988. Mechanism of spontaneous inside-out vesiculation of red cell membranes. *J. Cell Biol.* 106:1893–1901.

17. Deguercy, A., M. Hommel, and J. Schrével. 1990. Purification and characterization of 37-kilodalton proteases from *Plasmodium falciparum* and *Plasmodium berghei* which cleave erythrocyte cytoskeletal components. *Mol. Biochem. Parasitol.* 38:233–244.

18. Millholland, M. G., R. Chandramohanadas, A. Pizzarro, A. Wehr, H. Shi, C. Darling, C. T. Lim, and D. C. Greenbaum. 2011. The malaria parasite progressively dismantles the host erythrocyte cytoskeleton for efficient egress. *Mol. Cell. Proteomics.* 10: M111.010678.

19. Tu, Z. C., and Z. C. Ou-Yang. 2003. Lipid membranes with free edges. *Phys. Rev. E Stat. Nonlin. Soft Matter Phys.* 68:061915.

20. Karatekin, E., O. Sandre, …, F. Brochard-Wyart. 2003. Cascades of transient pores in giant vesicles: line tension and transport. *Biophys. J.* 84:1734–1749.

21. Heinrich, V., K. Ritchie, …, E. Evans. 2001. Elastic thickness compressibilty of the red cell membrane. *Biophys. J.* 81:1452–1463.

22. Rawicz, W., K. C. Olbrich, …, E. Evans. 2000. Effect of chain length and unsaturation on elasticity of lipid bilayers. *Biophys. J.* 79:328–339.

23. Kamien, R. D. 2002. The geometry of soft materials: a primer. *Rev. Mod. Phys.* 74:953–971.

24. Douezan, S., M. Wyart, …, D. Cuvelier. 2011. Curling instability induced by swelling. *Soft Matter.* 7:1506–1511.

25. Reyssat, E., and L. Mahadevan. 2011. How wet paper curls. *Europhys. Lett.* 93:54001.

26. Callan-Jones, A. C., P.-T. Brun, and B. Audoly. 2012. Self-similar curling of a naturally curved elastica. *Phys. Rev. Lett.* 108:174302.

27. Reference deleted in proof.

28. Guyon, E., J.-P. Hulin, …, C. Mitescu. 2001. Physical Hydrodynamics. Oxford University Press, Oxford, United Kingdom.

29. Verberg, R., I. M. de Schepper, and E. G. D. Cohen. 1997. Viscosity of colloidal suspensions. *Phys. Rev. E Stat. Phys. Plasmas Fluids Relat. Interdiscip. Topics.* 55:3143–3158.

30. Evans, E. A. 1983. Bending elastic modulus of red blood cell membrane derived from buckling instability in micropipet aspiration tests. *Biophys. J.* 43:27–30.

31. Reference deleted in proof.

32. Reference deleted in proof.

33. Dimova, R., C. Dietrich, A. Hadjiisky, K. Danov, and B. Pouligny. 1999. Falling ball viscosimetry of giant vesicle membranes: finite-size effects. *Eur. Phys. J. B*. 12:589–598.

34. Hochmuth, R. M., P. R. Worthy, and E. A. Evans. 1979. Red cell extensional recovery and the determination of membrane viscosity. *Biophys. J.* 26:101–114.

35. Brochard, F., and J. F. Lennon. 1975. Frequency spectrum of the flicker phenomenon in erythrocytes. *J. Phys.* 36:1035.

36. Gov, N., A. G. Zilman, and S. Safran. 2003. Cytoskeleton confinement and tension of red blood cell membranes. *Phys. Rev. Lett.* 90:228101.

37. Rochal, S. B., and V. L. Lorman. 2006. Cytoskeleton influence on normal and tangent fluctuation modes in the red blood cells. *Phys. Rev. Lett.* 96:248102.

38. Lenormand, G., S. Hénon, …, F. Gallet. 2001. Direct measurement of the area expansion and shear moduli of the human red blood cell membrane skeleton. *Biophys. J.* 81:43–56.